OXFORD

Cerebral Cortex, 2024, **34**, bhae065
https://doi.org/10.1093/cercor/bhae065
Advance access publication date 9 March 2024
Original Article

Utilizing graph convolutional networks for identification of mild cognitive impairment from single modal fMRI data: a multiconnection pattern combination approach

Jie He[1,2,†], Peng Wang[3,4,†], Jun He[5], Chenhao Sun[6], Xiaowen Xu[7,8], Lei Zhang[1], Xin Wang[5,*], Xin Gao[2,*]

[1]School of Mathematics and Statistics, Chongqing Jiaotong University, Chongqing 400074, China
[2]Department of PET/MR, Shanghai Universal Medical Imaging Diagnostic Center, Shanghai 200233, China
[3]Department of Radiology, Shanghai 411 Hospital, Shanghai 200080, China
[4]RongTong Medical Healthcare Group Co. Ltd., Shanghai 20080, China
[5]College of Information Science and Technology, Chongqing Jiaotong University, Chongqing 400074, China
[6]Department of Radiology, Rugao Jian'an Hospital, Rugao, Jiangsu 226500, China
[7]Tongji University School of Medicine, Tongji University, Shanghai 200092, China
[8]Department of Medical Imaging, Tongji Hospital, Shanghai 200092, China

*Corresponding authors: Email: WangX_003@163.com (Xin Wang); Email: gaoxin@uvclinic.cn (Xin Gao)
†Jie He and Peng Wang contributed to this paper equally.

Mild cognitive impairment plays a crucial role in predicting the early progression of Alzheimer's disease, and it can be used as an important indicator of the disease progression. Currently, numerous studies have focused on utilizing the functional brain network as a novel biomarker for mild cognitive impairment diagnosis. In this context, we employed a graph convolutional neural network to automatically extract functional brain network features, eliminating the need for manual feature extraction, to improve the mild cognitive impairment diagnosis performance. However, previous graph convolutional neural network approaches have primarily concentrated on single modes of brain connectivity, leading to a failure to leverage the potential complementary information offered by diverse connectivity patterns and limiting their efficacy. To address this limitation, we introduce a novel method called the graph convolutional neural network with multimodel connectivity, which integrates multimode connectivity for the identification of mild cognitive impairment using fMRI data and evaluates the graph convolutional neural network with multimodel connectivity approach through a mild cognitive impairment diagnostic task on the Alzheimer's Disease Neuroimaging Initiative dataset. Overall, our experimental results show the superiority of the proposed graph convolutional neural network with multimodel connectivity approach, achieving an accuracy rate of 92.2% and an area under the Receiver Operating Characteristic (ROC) curve of 0.988.

Key words: functional network; mild cognitive impairment; graph convolutional neural network; resting-state fMRI; brain connectivity network.

Introduction

Alzheimer's disease (AD) is a neurodegenerative disorder and it is the predominant cause of dementia worldwide (Breijyeh and Karaman 2020). It is characterized by a gradual deterioration in cognitive functions, and it predominantly impacts the elderly population, with an incidence rate that doubles every 5 years once the individuals reach the age of 60 (Bain et al. 2008). However, despite extensive research, identifying efficacious therapeutic approaches for AD remains challenging. Thus, an early intervention to decelerate its advancement holds paramount importance for improved patient treatment and care.

Mild cognitive impairment (MCI), widely acknowledged as a precursor to AD, has garnered substantial attention in medical research (Wee et al. 2012). It represents an early stage of cognitive decline, with approximately 10%–15% of individuals diagnosed with MCI progressing to AD each year (Misra et al. 2009), highlighting the pressing need for the precise and timely MCI diagnosis as a strategic approach to potentially delay or prevent the onset of AD. Given the absence of curative treatments, current efforts primarily concentrate on pharmacological and behavioral interventions during the initial stages of the disease, with the aim of alleviating symptoms and enhancing the quality of life for affected individuals. Therefore, the early identification and management of both MCI and AD play a pivotal role in addressing this challenging and prevalent condition.

fMRI has recently emerged as an important modality for assessing brain activity (Yang et al. 2023), particularly in the evaluation of MCI (Kemik et al. 2023). Li et al. (2020) reported the increasing use of fMRI to identify distinctive brain patterns associated with MCI. In addition, several recent research studies have been carried out to explore the association between MCI and cerebral networks (Chen et al. 2021; Du et al. 2023). Nevertheless, challenges persist in the application of fMRI for MCI diagnosis due to the inherent variability and asynchrony in spontaneous brain activity across subjects and scanners, often complicating the differentiation between individuals with MCI and normal control (NC) groups.

To address this challenge, connectivity-based approaches have emerged as the predominant method for diagnosing MCI due to their capacity to identify more robust and informative biomarkers

Received: January 21, 2024. **Revised:** January 31, 2024. **Accepted:** February 1, 2024

for understanding brain function (Stam 2014) by primarily concentrating on the intricate mapping and analysis of brain connections that underpin its functioning. Extensive research in this domain has consistently indicated strong associations between alterations in the functional connectivity and various neurological disorders. Notably, investigations by Chen et al. (2016) on AD, Gao et al. (2020) on MCI, Li et al. (2017) on autism spectrum disorders, and Baggio et al. (2014) on Parkinson's disease all reported the pivotal role played by brain functional connectivity in these pathological conditions. In addition, accumulating evidence suggests that connectivity-based approaches offer a more dependable and comprehensive comprehension of neurodegenerative diseases while also unveiling new insights for diagnosis and potentially influencing treatment strategies.

To effectively use the functional brain network (FBN) in neurodisease diagnosis, graph convolutional neural networks (GCN) have been applied to enhance the accuracy of disease diagnosis (Lu and Uddin 2023). This approach revolves around the fundamental concept of treating each brain network as a graph, with nodes representing distinct brain regions and edges denoting their functional connections (Zhang M et al; Zhang X et al; Saeidi et al. 2022; Ma et al. 2023; Wu et al. 2020; Wu et al. 2022). However, prior GCN studies have mostly focused on analyzing the topological characteristics and connection strengths of FBN based on specific connectivity patterns while neglecting other connection patterns. However, the gap in our understanding leaves researchers questioning the potential additional information that different connection patterns within the FBN may offer.

In this regard, we integrated GCN with the multimodal connectivity approach proposed in previous research for diagnosing MCI (Li et al. 2021) by utilizing GCN to extract and combine features from various modes, including full correlation, partial correlation, and causality patterns, thereby enhancing the synergistic advantages derived from their combination.

To evaluate the effectiveness of our approach, we conducted experiments using the Alzheimer's Disease Neuroimaging Initiative (ADNI) dataset, which comprised 92 subjects. Importantly, we employed 3 models—Pearson's correlation (PC), sparse representation (SR), and Granger causality mapping (GCM)—to construct FBNs, capturing different modes of connectivity. Overall, our results demonstrated the superiority of integrating diverse connectivity patterns through GCN over models relying solely on the individual connectivity patterns (Wu et al. 2020; Wu et al. 2022). This improvement in diagnostic accuracy, particularly for MCI diagnosis, highlights the potential of our advanced neuroimaging technique in advancing the diagnosis of brain disorders. Additionally, we conducted a post hoc analysis to visualize significant nodes in GCN for MCI diagnosis and confirmed their biological relevance.

Material and methods

Data preparation

For this study, we accessed neuroimaging data from the widely recognized ADNI dataset (http:/adni.loni.ucla.edu), initially referenced by Jack et al. (2010), for our analysis and experiments. Our research specifically focused on a distinct subset of the ADNI database, comprising a total of 92 participants. Among these participants, 47 individuals were diagnosed with MCI, while the remaining 45 participants constituted the healthy NC group to ensure a balanced representation of both affected and healthy populations (Table 1), which includes their respective demographic information.

Table 1. Baseline characteristics of the investigated patients.

	MCI ($n = 47$)	NC ($n = 45$)
Gender (M/F)	19/28	18/27
Age (year ± SD)	73.0±5.32	73.1±5.65

MCI, mild cognitive impairment; NC, normal control.

The resting-state fMRI (rs-fMRI) is a specialized variant of fMRI that specifically investigates the brain's functional connectivity network during periods of rest (Meng and Ge. 2022). The rs-fMRI images were acquired using a standardized echo planar imaging protocol on the 3T Siemens Allegra scanner (Smith et al. 2011). During data acquisition, the participants were instructed to maintain a relaxed state and focus their attention on a white cross displayed against a black background on the screen for the entire 6-min scanning session. This experimental setup was designed to minimize potential interference from external stimuli and to reduce motion artifacts. To optimize the data quality, we used the following specific imaging parameters: a flip angle of 90°, 33 slices per brain volume, a repetition time of 2,000 ms, and an echo time of 15 ms. We obtained a total of 180 volumes, with each voxel having a thickness of 4.0 mm. These carefully selected parameters ensured an optimal balance between the spatial and temporal resolutions, which is crucial for the precise analysis of the functional connectivity.

To preprocess the data, we utilized the widely adopted Statistical Parameter Mapping software (SPM8) (http://www.fil.ion.ucl.ac.uk.spm), a standard tool in neuroimaging. To address potential signal artifacts, we excluded the initial 10 volumes from each subject's dataset. Subsequent preprocessing steps involved: (i) aligning the images with the Montreal Neurological Institute standard space to compare the subjects; (ii) integrating Friston's 24-parameter model (Friston et al. 1996) into regression analysis to account for physiological and motion-related artifacts; (iii) applying a band-pass filter with a frequency range of 0.01–0.08 Hz to focus on resting-state fluctuations within specific frequency bands; and finally (iv) detrending the signal by eliminating its linear trend component. After preprocessing, the BOLD time series signals were segmented into 116 regions of interest (ROIs) based on the Automated Anatomical Labeling (AAL) atlas (Rolls et al. 2020). These time series were then organized into a data matrix represented as $\boldsymbol{X} \in \boldsymbol{R}^{170\times116}$ to further analyze the functional connectivity patterns and network dynamics in the brain.

Each of the mentioned data preprocessing steps has significant implications: (i) spatial normalization ensures consistency in the spatial patterns across subjects' images and reduces individual differences, thus enabling analysis at a group level; (ii) motion correction was conducted using Friston's 24-parameter model to eliminate artifacts caused by head movement. Head motion introduces noise into fMRI data, which needs to be corrected for obtaining reliable brain activity information; (iii) band-pass filtering was applied within the frequency range of 0.01–0.08 Hz to focus on the specific functional frequency bands of the brain. Different frequency bands represent the neural activity at different scales, and this step assists in extracting functional information from targeted frequency ranges; (iv) detrending eliminates the linear trend component from the signal, removing low-frequency drift influence and resulting in cleaner functional data; (v) brain region segmentation involves dividing the image into 116 ROIs for subsequent analysis based on regional time series, facilitating the examination of connectivity patterns at a regional level (Tzourio–Mazoyer et al. 2002).

Multimode graph construction

The graph G, referred to as $G = \{V, E, A\}$, represents a group of nodes or ROIs comprising n elements in V, the set of edges in E, and A as the adjacency matrix in $R^{n\times n}$. It characterizes the connections between specific FBN nodes or ROIs. Our research protocol was to conduct PC, SR and GCM as the FBN construction model to measure different connection patterns, including the full correlation, partial correlation, and causality between ROI.

Pearson's correlation

PC coefficient is commonly utilized for estimating FBNs due to its simplicity and intuitive nature, and it is 1 of the 3 connectivity patterns for constructing brain networks based on the AAL atlas. Using t to represent the total number of time points or steps, $\bar{x}_i \in R^t$ to denote the average calculated from all elements in the vector $x_i\ (i = 1, 2, \cdots, n)$, $x_i - \bar{x}_i$ to represent the centralized counterpart of x_i, and $x_i \in R^t$ to represent BOLD signal sequences derived from each respective ROI, we could determine the connection weight w_{ij} that links 2 ROIs.

$$W_{ij} = \frac{(x_i - \bar{x}_i)^T (x_j - \bar{x}_j)}{\sqrt{(x_i - \bar{x}_i)^T (x_i - \bar{x}_i)}\sqrt{(x_j - \bar{x}_j)^T (x_j - \bar{x}_j)}}, \quad (1)$$

where w_{ij} represents the connection weights of the ith and the jth ROI.

Sparse representation

The SR technique is a modeling approach for partial correlations. Compared to PC, which measures the overall correlation across ROIs, partial correlation involves eliminating the confounding effects of other ROIs (Huang et al. 2010). The SR model, as described in previous research (Li et al. 2019), can be summarized as follows:

$$\min_W \sum_{i=1}^{n} \left\| x_i - \sum_{j\neq i} W_{ij} x_j \right\|^2 + \lambda \sum_{j\neq i} |W_{ij}|. \quad (2)$$

The matrix form is proposed as follows:

$$\min_W \|X - XW\|_F^2 + \lambda \|W\|_1$$
$$\text{s.t.} W_{ii} = 0, \forall i = 1, \cdots, n. \quad (3)$$

The data for a particular individual's fMRI is denoted by the matrix $X = [x_1, x_2, \cdots, x_n] \in R^{t\times n}$.

Granger causality mapping

GCM is a technique used to model the effective connectivity of networks, with the goal of identifying the causal influence between network nodes. In contrast to methods that assume symmetrical interactions, GCM emphasizes the asymmetrical nature of these connections, providing a more nuanced comprehension of directional effects within the network. Specifically, when examining 2 time series, $x[n]$ and $y[n]$, the Granger causal mapping from $x[n]$ to $y[n]$ can be expressed in the following manner:

$$F_{x,y} = \ln \frac{|\sum(\zeta_t)|}{|\sum(\eta_t)|}. \quad (4)$$

The parameter ζ_t is used to constrain the regression model's residual error, while η_t is employed for an unconstrained regression model's residual error. The symbol Σ represents the variance.

Multimode connections introducing graph convolution

In this present study, we introduce a unique method for examining FBNs by constructing multimodal graphs for each participant (Fig. 1). This approach involves dividing the brain into 116 ROIs based on the AAL atlas developed by Rolls et al. (2020). To identify diverse patterns of brain connectivity, we utilize 3 distinct types of connectivity measures: PC, SR, and GCM, with each measure offering a unique insight into the brain function and enabling a comprehensive analysis. We also used multiple graph GCN modules to effectively obtain the distinctive characteristics associated with each type of connectivity pattern and to generate a multimodal graph representation for each subject, which is subsequently integrated to determine the collective strengths of various connectivity patterns and enhance the overall feature representation. Subsequently, these multimodal features are consolidated through 3 fully connected layers during processing. The output from the final layer forms the foundation of our disease classification algorithm, specifically designed for diagnosing particular conditions. Significantly, our study stands out as pioneering research by introducing GCNs across various modalities while constructing multimodal connections for MCI diagnosis.

In this section, we consider FBNs as heterogeneous graphs with intricate internal structures. To investigate these FBNs and to generate novel graph representations for improving the diagnosis of MCI, we employed a spectral GCN approach based on the framework proposed by Zhang et al. (2018). Expanding upon the previous work of Bruna et al. (2013) and Kawahara et al. (2017), spectral GCN effectively captures the internode information in the spectral domain through Fourier transform and its inverse.

The Fourier transform of a graph heavily depends on the Laplacian matrix L, which is denoted as $L = D - A$. In this formulation, the diagonal elements D_{ij} of the diagonal matrix D correspond to the degree of node i. Specifically, D_{ij} represents the total weight of all edges connected to node i, and it can be expressed as $D_{ii} = \sum_j A_{ij}$. A frequently used variation of the Laplacian matrix is known as the normalized symmetric Laplacian matrix and can be expressed as follows:

$$L = D^{-1/2} L D^{-1/2} = I_n - D^{-1/2} A D^{-1/2}, \quad (5)$$

where I_n is an identity matrix.

The Laplacian matrix L can be factorized as $U\Lambda U^T$, where $U = \{u_i\}_{i=1}^n$ represents a set of orthogonal eigenvectors and $\Lambda = \text{diag}(\{\alpha_i\}_{i=1}^n)$ denotes a diagonal matrix consisting of eigenvalues α_i, which simplifies the conversion of variables into the spectral domain, facilitating convolution operations on graphs (Kipf and Welling 2016).

In each pattern graph, we incorporate 2 convolutional layers and employ ReLU as the activation function. Then, we apply the forward propagation formula:

$$f(X, A) = \text{ReLU}\left[\hat{A}\,\text{ReLU}\left(\hat{A} X W^{(0)}\right) W^{(1)}\right]. \quad (6)$$

Herein, the dimension of the output feature is denoted by $f(X, A) \in R^{n\times d}$, where $X \in \{X_{PC}, X_{SR}, X_{GCM}\}$ and $A \in \{A_{PC}, A_{SR}, A_{GCM}\}$ and $\hat{A} = A + I_n$. The matrix $W^{(0)}$ represents the adjustable weights of the first convolutional layer, while $W^{(1)}$ is the parameter matrix for the weights of the second convolutional layer.

The final class label prediction in this study was based on the GCN model, as previously reported. To generate fixed-length

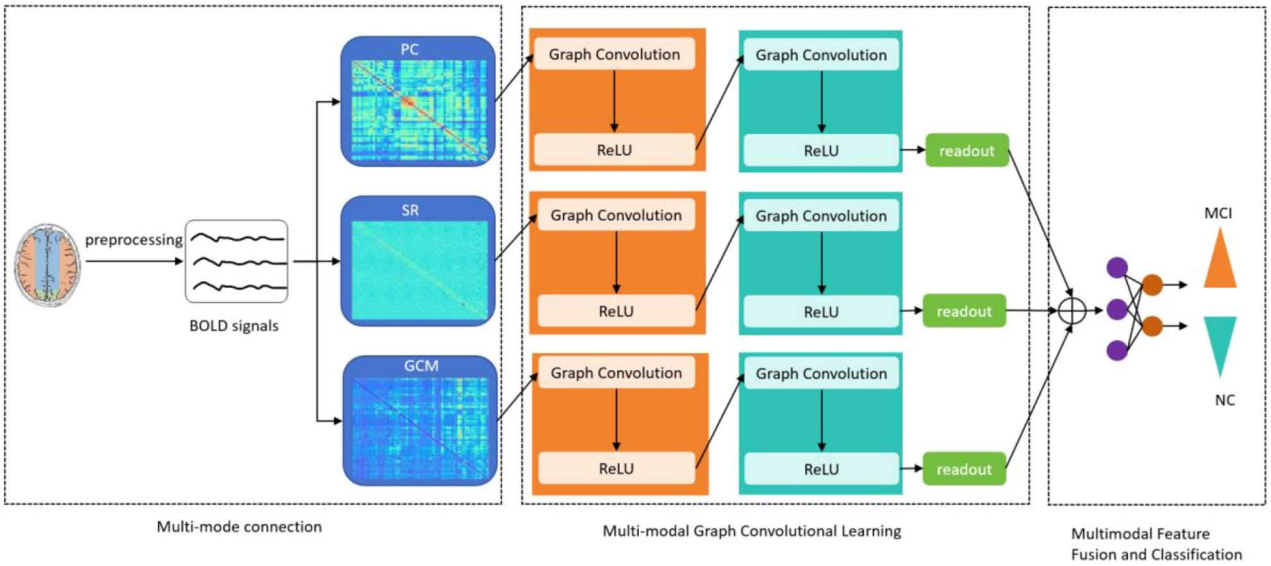

Fig. 1. GCNMC framework diagram for diagnosing MCI.

vectors describing 3 distinct patterns from an individual and combine node features, we employed a combination of Max pooling and average pooling operations. The readout layer is defined as shown in the equation below, following the approach of Lee et al. (2019):

$$F = \frac{1}{n}\sum_{i=1}^{N} f_i(X, A) \left\| \max_{i=1}^{N} f_i(X, A) \right. . \tag{7}$$

The convolution algorithm utilized by $f_i(X, A)$ is used to obtain the ROI, and subsequently, the merge operation $\|$ is utilized to combine the feature vectors from each ROI into a unified vector.

Implementation details

Our PyTorch-based model efficiently utilizes the NVIDIA GeForce RTX 4090 GPU with 16 GB of video memory. It incorporates 2 GCN modules, each processing 3 types of connections separately for feature extraction. These features are then passed through a fully connected layer for classification. To optimize the model, we used the Adam optimizer (Kingma and Ba 2014) with a learning rate of 0.025 and a regularization parameter of 0.00001 during 150 training epochs.

Experiments and results

The brainnetclass toolbox, as established in previous studies (Zhou et al. 2020), is widely employed for estimating PC and SR. To determine the hyperparameters of SR, Leave-One-Out Crossvalidation is commonly used. In Fig. 2, the accuracy of different hyperparameters is illustrated, and after a comparative analysis, $\lambda = 2^0$ is selected. Additionally, for the estimation of GCM, we utilize the dynamic BC toolbox (Liao et al. 2014).

Visualization of brain network matrix estimation for a single modality

Figure 3 shows the connectivity matrices of the FBN using various connection techniques and highlights the distinctive brain network topologies associated with the PC, SR, and GCM methods.

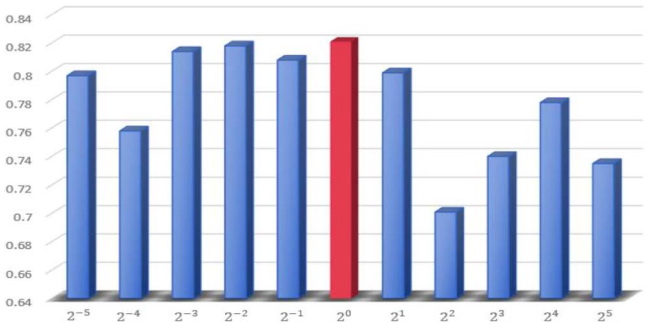

Fig. 2. The accuracy of the SR model with varying hyperparameter λ.

Comparative analysis

Our proposed approach was compared using 2 distinct connectivity patterns: a single connection pattern and a partial connection pattern. In the single connection pattern, 3 methods were used: (i) the construction of a brain network using PC, (ii) the creation of a brain network through SR, and (iii) the establishment of a brain network using GCM. Conversely, the partial connectivity patterns involve pairwise combinations of these individual connectivity methods, encompassing: (iv) the fusion of PC and SR for brain network construction, (v) the combination of PC and GCM for brain network development, and (vi) the combination of SR and GCM to construct the brain network.

Classification results

The training set was constructed by randomly selecting 70% of the samples, followed by an additional random selection of 10% for the validation set, leaving the remaining 20% for the test set. During each training iteration, parameters were saved at their peak performance level while also recording the average evaluation results and their SD. To ensure the fairness of our experiments, we assessed performance under consistent data partitioning and training strategies. Moreover, a comprehensive evaluation of the model was conducted using 5 key metrics: accuracy, recall, precision, F1-Score, and the area under the ROC

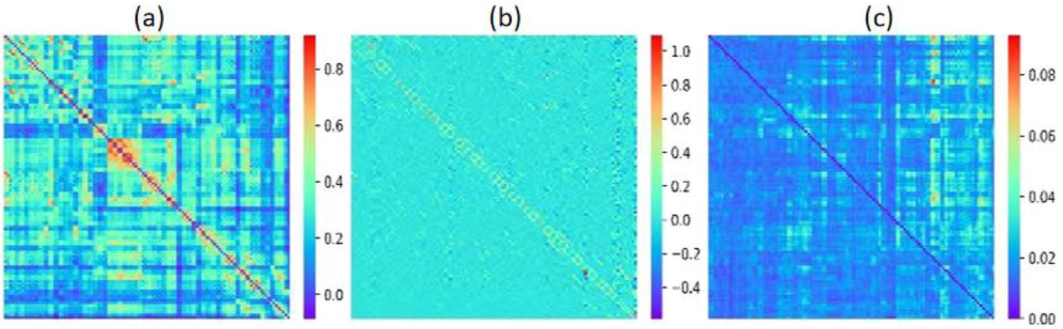

Fig. 3. The connectivity networks generated by a) PC, b) SR, and c) GCM methods.

curve (AUC) using the following equations:

$$\text{Accuracy} = \frac{\text{TP} + \text{TN}}{\text{TP} + \text{FN} + \text{FP} + \text{TN}}, \tag{8}$$

$$\text{Precision} = \frac{\text{TP}}{\text{TP} + \text{FP}}, \tag{9}$$

$$\text{Recall} = \frac{\text{TP}}{\text{TP} + \text{FN}}, \tag{10}$$

$$F1 - \text{Score} = \frac{2 * \text{Precision} * \text{Recall}}{\text{Precision} + \text{Recall}}. \tag{11}$$

In these formulas, TP signifies the number of correctly identified samples with MCI, TN represents the accurately identified samples without MCI, FP indicates the incorrectly identified samples as having MCI, and FN denotes the incorrectly identified samples as not having MCI. Additionally, ROC curves can be plotted using the *X*-axis to depict the false positive rate (FPR) and the *Y*-axis to represent the true positive rate (TPR). FPR, TPR, and ROC are calculated as follows:

$$\text{FPR} = \frac{\text{TP}}{\text{TP} + \text{FN}}, \text{TPR} = \frac{\text{FP}}{\text{FP} + \text{TN}}. \tag{12}$$

The AUC is obtained by integrating the ROC curve, and the value obtained by this integral is the AUC value. The AUC quantifies the likelihood of a classifier ranking a randomly selected positive case higher than a randomly selected negative case, whereby a higher AUC value indicates a greater ability of the model to distinguish between cases, with values closer to 1 signifying a stronger predictive power.

We started by integrating GCN into the brain networks constructed using the PC, SR, and GCM methods to generate the first 3 single-mode connected brain networks for comparative analysis. Our proposed GCN module comprises 2 convolutional layers and a readout layer. Following the application of the convolutional layers, the data were assessed through a fully connected layer, culminating in the final classification achieved through 2 neurons in the last layer. Subsequently, we combined these established single-mode connected brain networks pairwise, maintaining identical parameter settings to create 3 additional types of brain networks. The experimental results are shown in Table 2, and Fig. 3 illustrates the corresponding ROC curve.

The comparison of the evaluation metrics and the ROC curve between the single-mode connection mode and the partial connection mode showed the following key findings:

(1) Based on the findings presented in Table 2, it is clear that PC_SR_GCM consistently achieves the highest evaluation scores, all of which are >0.9 except for Recall. As depicted in Fig. 3, GCM demonstrates a relatively weaker performance compared to other models, while PC_SR_GCM exhibits the strongest performance among all considered models. However, when comparing unimodal models, PC emerges as the most dominant model with a superior performance than PC_GCM.

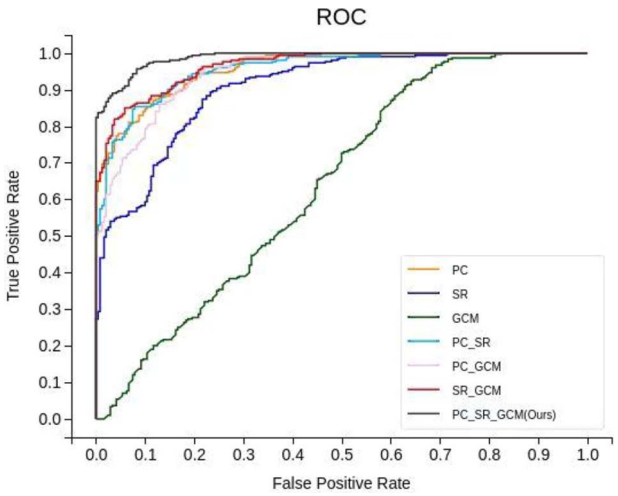

Fig. 4. ROC curves for the 7 connection modes.

(2) Combining connectivity data from both modes yields significant advantages compared to using a single model, highlighting the effectiveness of incorporating diverse connectivity models. Moreover, as the number of connectivity approaches increases, there is a clear trend toward progressive improvement in performance.

(3) The model's efficiency is further affirmed by integrating 3 distinct connectivity patterns into the classifier, resulting in an overall enhancement of its effectiveness.

(4) After analyzing the results presented in Fig. 4, we observed that with an increasing number of fused connectivity patterns, the ROC curve gradually approaches that of the optimal model, and it could be primarily attributed to the use of various connectivity patterns within FBN features, which potentially encompass additional information used collectively to enhance classification outcomes.

FBN feature visualization

To explore the dispersion of FBN features obtained from various connectivity patterns in more detail, we applied the *t*-SNE algorithm (Van Maaten and Hinton 2008) to reduce the dimensions of FBN features derived from 7 distinct connectivity modes

Table 2. The classification results of various models for MCI.

Model	Acc	Precision	Recall	F1-score	AUC
PC	0.850±0.088	0.760±0.152	0.969±0.068	0.842 ± 0.099	0.959±0.000
SR	0.820±0.138	0.847±0.138	0.856 ±0.138	0.841±0.114	0.904 ±0.000
GCM	0.665± 0.125	0.897± 0.209	0.661±0.113	0.737±0.143	0.642±0.000
PC_SR	0.881±0.123	0.853 ±0.166	0.934±0.103	0.882 ±0.130	0.955±0.000
PC_GCM	0.869±0.153	0.900±0.146	0.905±0.157	0.888±0.126	0.948±0.000
SR_GCM	0.885±0.153	0.840±0.236	0.940 ±0.126	0.872 ±0.193	0.965 ±0.000
PC_SR_GCM	0.922± 0.132	0.959±0.086	0.897±0.204	0.914±0.164	0.988±0.000

MCI, mild cognitive impairment; AUC, area under the ROC curve; PC, Pearson's correlation; SR, sparse representation; GCM, Granger causality mapping.

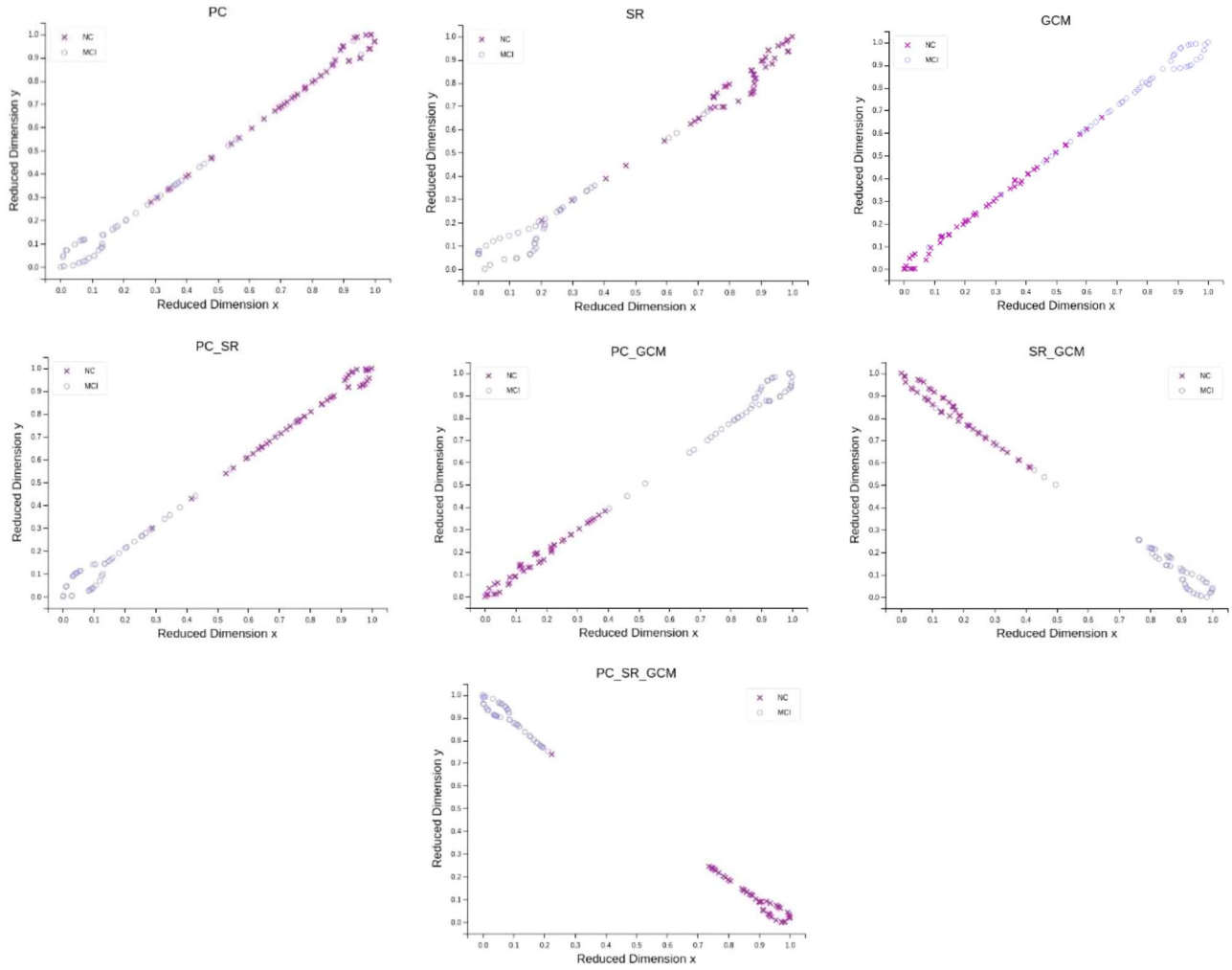

Fig. 5. The visualization of FBN features for 7 distinct connection modality methods.

into a 2D representation, as shown in Fig. 5. The results show that when 2 information modes are used, there is a more distinct separation among samples of different types compared to using just 1 mode. Furthermore, samples within the same category tend to cluster together more tightly, and this effect becomes even more pronounced when 3 information modes are incorporated. Collectively, as the number of fused connections increases, this trend becomes more prominent.

Significant nodes

In our present study, the input data consist of brain region node graphs for all patients, and to identify the nodes that significantly contribute to the diagnostic results of MCI, we employed a 2-step process. Initially, the nodes underwent forward propagation to obtain their activation values. Then, based on the magnitude of their contributions, we determined the nodes' indices based on the concept of Grad Cam (Selvaraju et al. 2020). The model's trained output comprises activation values for the nodes, which are processed through a softmax function. Unlike the previous experiments, this is a brand new experiment, so we replaced the activation function with a softmax function based on the existing experiment. Figure 6 illustrates the top 10% of nodes, while additional details regarding the gradient values of each node can be found in the Supplementary Materials.

As observed, the most significant nodes are primarily situated in areas, such as the precuneus, supplementary motor cortex,

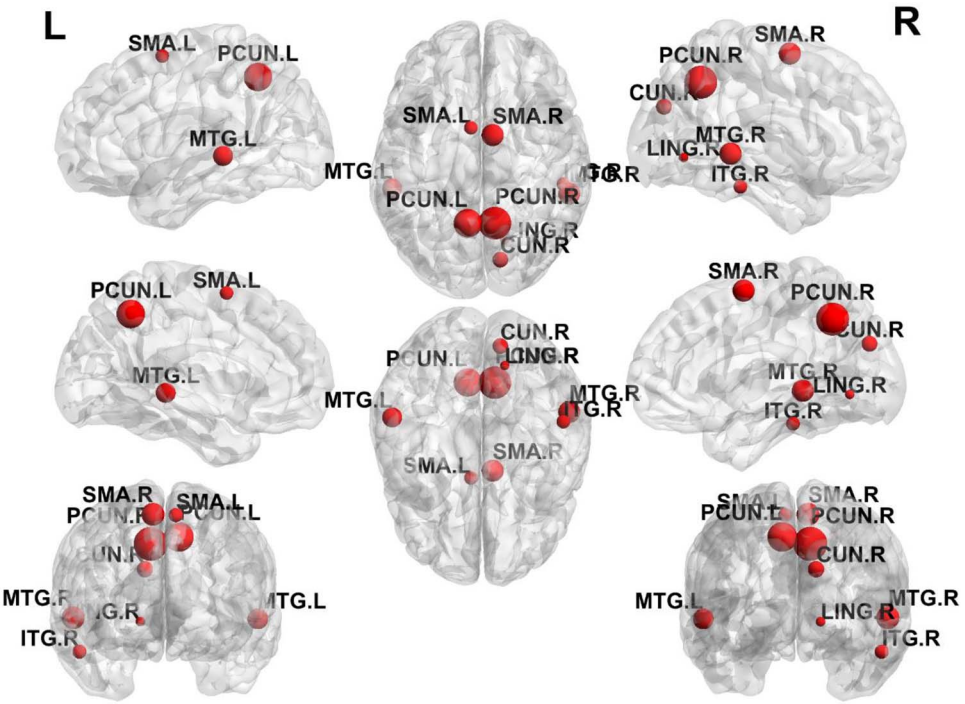

Fig. 6. The significant nodes for diagnosing MCI.

and middle temporal gyrus and cuneus, all of which are closely associated with MCI, which provides further confirmation of the effectiveness of our methods (Dong et al. 2021; Mattioli et al. 2021; Koppelmans et al. 2022).

Discussion

The PC model quantifies the linear correlation between time series of distinct brain regions, effectively capturing comprehensive information on functional connectivity. The SR mode facilitates the identification of specific connectivity patterns by eliminating the influence of other brain regions and focusing solely on partial correlations between 2 regions. The GCM model emphasizes causal relationships among different brain regions, providing directed connection information and offering unique advantages in understanding the connection causality. Multimodal integration enables harnessing the strengths of diverse connectivity patterns, resulting in a more comprehensive and accurate representation of the brain functional connectivity through integrating various types of connectivity information.

The experimental results demonstrate that, within the context of a single-mode connection model, the PC method outperforms the SR and GCM methods in terms of accuracy. Incorporating information from a single pattern leads to a substantial improvement in the model performance, which becomes even more pronounced with the combination of multiple patterns. Furthermore, the validation of our proposed approach through the pairwise combination of different patterns further confirms its superiority. Thus, our multimodal connection method, which introduces a fusion of various connections based on GCN, significantly enhances the diagnostic accuracy of MCI. Moreover, the utilization of multiple connection modes may enable us to capture diverse discriminant information for diagnostic purposes.

Conclusion

In conclusion, we introduce an innovative approach for diagnosing MCI using unimodal rs-fMRI data to harness the power of GCNs in enhancing the classification capabilities of a single modality. We also integrate the data features processed by GCNs with different connection patterns and input them into a neural network for feature fusion. With the utilization of just 2 neurons, the disease diagnosis could be successfully achieved. To assess the effectiveness of our approach, we conducted experiments using the ADNI database, validating the efficacy of our graph convolutional neural network with multimode connectivity (GCNMC). Taken together, our results show that GCNMC excels in learning FBN features and effectively diagnosing MCI.

Additionally, the study has successfully identified key brain regions associated with the diagnosis of MCI, including the precuneus, supplementary motor area, middle temporal gyrus, and cuneus, through meticulous visual analysis. This novel insight into the neural mechanisms underlying MCI offers valuable implications. Furthermore, this method solely requires single-mode fMRI data and boasts of user-friendly operation procedures, thus providing a practical tool for diagnosing MCI. Consequently, this study serves as a significant reference for utilizing GCNs with multimode connections in diagnosing other neurological disorders.

Author contributions

Jie He (Methodology, Writing—original draft), Peng Wang (Validation, Writing—original draft), Jun He (Writing—original draft), Chenhao Sun (Investigation, Validation), Xiaowen Xu (Supervision, Writing—original draft, Writing—review & editing), Lei Zhang (Writing—review & editing), Xin Wang (Investigation, Writing—review & editing), and Xin Gao (Visualization, Writing—review & editing).

Supplementary material

Supplementary material is available at *Cerebral Cortex* online.

Funding

This study was funded by National Natural Science Foundation of China (62306051, 82102023, 81830059, and 82227807); Shanghai Committee of Science and Technology Project (21Y11906100); Research Project of Shanghai Municipal Health Commission (20224Y0340 and 2022JC017); Joint Training Base Construction Project for Graduate Students in Chongqing (JDLHPYJD2021016); Group Building Scientific Innovation Project for Universities in Chongqing (CXQT21021); The Science and Technology Research Program of Chongqing Municipal Education Commission (KJQN202300718); Open Program of Hubei Province Key Laboratory of Molecular Imaging (2023fzy023); and Scientific Research Subjects of Shanghai Universal Medical Imaging Technology (UV2021Z01, UV2022M06, and UV2023Z01).

Conflict of interest statement: None declared.

Data availability

All data generated or analyzed during this study are included in this published article.

Ethics approval and consent to participate

This study was approved by the Institution's Ethical Committee of Shanghai Mental Health Center of Shanghai Jiao Tong University School of Medicine. Written informed consent was obtained from individual or guardian participants.

Consent for publication

Not applicable.

References

Baggio HC, Sala-Llonch R, Segura B, Marti MJ, Valldeoriola F, Compta Y, Tolosa E, Junqué C. Functional brain networks and cognitive deficits in Parkinson's disease. *Hum Brain Mapp*. 2014:35(9):4620–4634.

Bain LJ, Jedrziewski K, Morrison-Bogorad M, Albert M, Cotman C, Hendrie H, Trojanowski JQ. Healthy brain aging: a meeting report from the sylvan M. Cohen annual retreat of the University of Pennsylvania Institute on aging. *Alzheimers Dement*. 2008:4(6):443–446.

Breijyeh Z, Karaman R. Comprehensive review on Alzheimer's disease: causes and treatment. *Molecules*. 2020:25(24):5789.

Bruna J, Zaremba W, Szlam A, LeCun Y. Spectral networks and locally connected networks on graphs. 2013, arXiv preprint arXiv:1312.6203.

Chen G, Shu H, Chen G, Ward BD, Antuono PG, Zhang Z, Li SJ. Staging Alzheimer's disease risk by sequencing brain function and structure, cerebrospinal fluid, and cognition biomarkers. *J Alzheimer's Dis*. 2016:54(3):983–993.

Chen H, Zhang Y, Zhang L, Qiao L, Shen D. Estimating brain functional networks based on adaptively-weighted fMRI signals for MCI identification. *Front Aging Neurosci*. 2021:12:595322.

Dong Q-Y, Li T-R, Jiang X-Y, Wang X-N, Han Y, Jiang J-H. Glucose metabolism in the right middle temporal gyrus could be a potential biomarker for subjective cognitive decline: a study of a Han population. *Alzheimers Res Ther*. 2021:13(1):74.

Du Y, Wang G, Wang C, Zhang Y, Xi X, Zhang L, Liu M. Accurate module induced brain network construction for mild cognitive impairment identification with functional MRI. *Front Aging Neurosci*. 2023:15:1101879.

Friston KJ, Williams S, Howard R, Frackowiak RSJ, Turner R. Movement-related effects in fMRI time-series. *Magn Reson Med*. 1996:35(3):346–355.

Gao X, Xu X, Hua X, Wang P, Li W, Li R. Group similarity constraint functional brain network estimation for mild cognitive impairment classification. *Front Neurosci*. 2020:14:165.

Huang S, Li J, Sun L, Ye J, Fleisher A, Wu T, Chen K, Reiman E, Alzheimer's Disease NeuroImaging Initiative. Learning brain connectivity of Alzheimer's disease by sparse inverse covariance estimation. *NeuroImage*. 2010:50(3):935–949.

Jack CR, Bernstein MA, Fox NC, Thompson P, Alexander G, Harvey D, Borowski B, Britson PJ, L. Whitwell J, Ward C et al. The Alzheimer's disease neuroimaging initiative (ADNI): MRI methods. *J Magn Reson Imaging*. 2010:27:685–691.

Kawahara J et al. BrainNetCNN: convolutional neural networks for brain networks; towards predicting neurodevelopment. *NeuroImage*. 2017:146:1038–1049.

Kemik K, Ada E, Çavuşoğlu B, Aykaç C, Emek-Savaş DD, Yener G. Functional magnetic resonance imaging study during resting state and visual oddball task in mild cognitive impairment. *CNS Neurosci Ther*. 2023:30(2):cns.14371.

Kingma DP, Ba J.APA. Adam: a method for stochastic optimization. 2014. https://doi.org/10.48550/arXiv.1412.6980.

Kipf TN, Welling MJAPA. Semi-supervised classification with graph convolutional networks. 2016. https://doi.org/10.48550/arXiv.1609.02907.

Koppelmans V, Silvester B, Duff K. Neural mechanisms of motor dysfunction in mild cognitive impairment and Alzheimer's disease: a systematic review. *J Alzheimer's Dis Rep*. 2022:6(1):307–344.

Lee J, Lee I, Kang J. Self-attention graph pooling. In: *International Conference on Machine Learning*. Long Beach, California: PMLR; 2019:3734–3743.

Li W, Wang Z, Zhang L, Qiao L, Shen D. Remodeling Pearson's correlation for functional brain network estimation and autism spectrum disorder identification. *Front Neuroinf*. 2017:11:55.

Li W, Zhang L, Qiao L, Shen D. Toward a better estimation of functional brain network for mild cognitive impairment identification: a transfer learning view. 2019:24(4):1160–1168.

Li W, Xu X, Jiang W, Wang P, Gao X. Functional connectivity network estimation with an inter-similarity prior for mild cognitive impairment classification. *Aging*. 2020:12(17):17328–17342.

Li W, Xu X, Wang Z, Peng L, Wang P, Gao X. Multiple connection pattern combination from single-mode data for mild cognitive impairment identification. *Front Cell Develop Biol*. 2021:9:782727.

Liao W, Wu GR, Xu Q, Ji GJ, Zhang Z, Zang YF, Lu G. DynamicBC: a MATLAB toolbox for dynamic brain connectome analysis. *Brain Connectivity*. 2014:4(10):780–790.

Lu H, Uddin S. Disease prediction using graph machine learning based on electronic health data: a review of approaches and trends. In healthcare. *MDPI*. 2023:11(7):1031.

Ma Y, Wang Q, Cao L, Li L, Zhang C, Qiao L, Liu M. Multi-scale dynamic graph learning for brain disorder detection with functional MRI. *IEEE Trans Neural Syst Rehabil Eng*. 2023:31:3501–3512.

Mattioli P, Pardini M, Famà F, Girtler N, Brugnolo A, Orso B, Meli R, Filippi L, Grisanti S, Massa F, et al. Cuneus/Precuneus as a central hub for brain functional connectivity of mild cognitive impairment in idiopathic REM sleep behavior patients. *Eur J Nucl Med Mol Imaging*. 2021:48(9):2834–2845.

Meng L, Ge KJBS. Decoding visual fMRI stimuli from human brain based on graph convolutional neural. *Network*. 2022:12(10):1394.

Misra C, Fan Y, Davatzikos C. Baseline and longitudinal patterns of brain atrophy in MCI patients, and their use in prediction of short-term conversion to AD: results from ADNI. *Alzheimers Dement*. 2009:44:1415–1422.

Rolls ET, Huang C-C, Lin C-P, Feng J, Joliot M. Automated anatomical labelling atlas 3. *NeuroImage*. 2020:206:116189.

Saeidi M, Karwowski W, Farahani FV, Fiok K, Hancock PA, Sawyer BD, Christov-Moore L, Douglas PK. Decoding task-based fMRI data with graph neural networks, considering individual differences. *Brain Sci*. 2022:12(8):1094.

Selvaraju RR, Cogswell M, das A, Vedantam R, Parikh D, Batra D. Grad-CAM: visual explanations from deep networks via gradient-based localization. *Int J Comput Vis*. 2020:128(2):336–359.

Smith SM, Miller KL, Salimi-Khorshidi G, Webster M, Beckmann CF, Nichols TE, Ramsey JD, Woolrich MW. Network modelling methods for FMRI. *NeuroImage*. 2011:54(2):875–891.

Stam, Cornelis J. Modern network science of neurological disorders. *Nature Reviews Neuroscience*. 2014:683–695.

Tzourio-Mazoyer N, Landeau B, Papathanassiou D, Crivello F, Etard O, Delcroix N, Mazoyer B, Joliot M. Automated anatomical labeling of activations in SPM using a macroscopic anatomical parcellation of the MNI MRI single-subject brain. *NeuroImage*. 2002:15(1):273–289.

Van der Maaten L, Hinton GJJOMLR. Visualizing data using t-SNE. 2008:9(11).

Wee CY, Yap PT, Zhang D, Denny K, Browndyke JN, Potter GG, Welsh-Bohmer KA, Wang L, Shen D. Identification of MCI individuals using structural and functional connectivity networks. *NeuroImage*. 2012:59(3):2045–2056.

Wu Z, Pan S, Chen F, Long G, Zhang C, Yu PS. A comprehensive survey on graph neural networks. *IEEE Trans Neural Netw Learning Syst*. 2020:32(1):4–24.

Wu S, Sun F, Zhang W, Xie X, Cui B. Graph neural networks in recommender systems: a survey. *ACM Comput Surv*. 2022:55(5):1–37.

Yang J, Xu X, Sun M, Ruan Y, Sun C, Li W, Gao X. Towards an accurate autism spectrum disorder diagnosis: multiple connectome views from fMRI data[J]. *Cereb Cortex*. 2023:34(1):bhad477.

Zhang D, Huang J, Jie B, Du J, Tu L, Liu M. Ordinal pattern: a new descriptor for brain connectivity networks. *IEEE Transactions on Medical Imaging*. 2018:37(7):1711–1722.

Zhang M, Cui Z, Neumann M, Chen Y. An end-to-end deep learning architecture for graph classification. In: *Proceedings of the AAAI Conference on Artificial Intelligence*. 2018a.

Zhang X, He L, Chen K, Luo Y, Zhou J, Wang F. n.d . Multi-view graph convolutional network and its applications on neuroimage analysis for Parkinson's disease. In: *AMIA Annual Symposium Proceedings*. American Medical Informatics Association; 2018b.

Zhou Z, Chen X, Zhang Y, Hu D, Qiao L, Yu R, Yap PT, Pan G, Zhang H, Shen D. A toolbox for brain network construction and classification (BrainNetClass). *Hum Brain Mapp*. 2020:41(10):2808–2826.